LASER INTERFEROMETER GRAVITATIONAL WAVE OBSERVATORY
- LIGO -
CALIFORNIA INSTITUTE OF TECHNOLOGY
MASSACHUSETTS INSTITUTE OF TECHNOLOGY

Document Type	**LIGO-T970097-01 - D**	2/4/98

Absorption in the Core Optics and LIGO Sensitivity

Bill Kells, Jordan Camp

Distribution of this draft:

LIGO Detector Group

This is an internal working note
of the LIGO Project..

California Institute of Technology
LIGO Project - MS 51-33
Pasadena CA 91125
Phone (818) 395-2129
Fax (818) 304-9834
E-mail: info@ligo.caltech.edu

Massachusetts Institute of Technology
LIGO Project - MS 20B-145
Cambridge, MA 01239
Phone (617) 253-4824
Fax (617) 253-7014
E-mail: info@ligo.mit.edu

WWW: http://www.ligo.caltech.edu/

n.

1 INTRODUCTION

The stored power levels in the intial LIGO are of the order 20 kW in the arms and 300 W in the recycling cavity. Absorption losses in the Core Optics at the level of 50 ppm bulk and 1 ppm surface will result in respective power deposits of tens of mW. The effect of the consequent thermal distortion of the optics is investigated in this note.

Sections 2 and 3 calculate the thermal distortion and effect on IFO sensitivity using order of magnitude estimates. These are compared with detailed simulations from the FFT code in section 4 which reveal other interesting physics of this problem.

2 THERMAL DISTORTION FROM ABSORBED POWER

The effect of absorbed power on an optic is seen in 2 ways: thermal expansion of the heated substrate and thermal lensing from a change in the substrate index of refraction. Both are due to the rise in temperature *dT* which accompanies the absorbed power, which is generated from losses in the coating and substrate. To 1st order, the distortion of the optic may be viewed as a variation in the sagitta *s*[1]:

$$\delta s \sim \frac{\alpha}{4\pi\kappa} P_a \text{ from thermal expansion}$$

where heating causes a physical deformation of the optic and where α is the thermal expansion coefficient, κ is the heat conductivity of the substrate, and P_a is the absorbed power. This may be compared with the nominal sag, $w_0^2 / 2R$ where R is the optic radius of curvature, and w_0 is the beam radius. The thermal expansion affects the mirror shape and is seen by both the beam transmitted through the substrate and the stored cavity beams incident on the surface. Also,

$$\delta s \sim \frac{\beta}{4\pi\kappa} P_a \text{ from thermal lensing,}$$

where heating causes a change in the substrate optical path and where $\beta = \frac{\partial n}{\partial T}$ with n the index of refraction. In the case of thermal lensing, the sag change is seen for the beam transmitted through the substrate.

Using the following constants for fused silica:

$$\alpha / \kappa = 3.3 \times 10^{-7} \text{ m / W}$$

1. Heating by optical absorption and the performance of interferometric gravitational-wave detectors, Winkler, Danzmann, Rudiger, and Schilling, Phys Rev A, Vol 44, 7022

$$\beta / \kappa = 1 \times 10^{-5} \text{ m / W}$$

we see that thermal lensing is the dominant effect. These expressions are accurate to within a factor of 2 for power absorbed directly in the coating or uniformly through the substrate.

With the interferometer power levels shown in table I, the following effective sag changes occur:

Table 1: Sag change in Core Optics

Optic	s_0 (nm)	Surface Power (Watt)	Bulk Power (Watt)	$\Delta s_{Expansion}$ (nm) L = 0.6 ppm	$\Delta s_{Lensing}$ (nm) L = 5 ppm / cm
RM	80	300	6	0.005	0.24
BS	0	300	150 (2x)	0.005	5
ITM	55	18000	150 (2x)	0.4	20
ETM	140	18000	0.5	0.3	(small)

We immediately see the seriousness of the effect in the ITM, where a total ~35% change in the sag from thermal lensing is found. For the above power and loss levels, surface and bulk absorption give comparable contributions to the ITM thermal lensing.

3 EFFECT ON IFO SENSITIVITY

We examine the effect of the sag changes on the stored carrier and sideband power, considering both the arm and recycling cavities. A change in sag is equivalent to a change in the optic radius of curvature; this results in a mode mismatch of the input light to the distorted cavity, causing a loss of stored power.

3.1. Arm Cavity

The arm cavity ITM undergoes an expansion sag change of ~1%, with the ETM ~0.2%. This gives a change in the waist size of ~0.2% and waist position of ~10 m, yielding a perturbation of the arm resonant mode with a ~0.1 % amplitude TEM_{02} term (relative to the fundamental). The resultant loss of stored power is negligible. Thus we can neglect the effect of the absorption on the cavity arm stored power.

3.2. Recycling Cavity

The recycling cavity is essentially unstable and gives no focusing of the circulating light. Both the recycling mirror and ITM are initially matched to the radius of curvature of the light *R* (set by mode matching the light to the arm cavity.) Thermal lensing of the ITM causes a change in its curvature, to R'. The modal composition of the light produced by reflection from the distorted optic can be written as:

$$\Psi(R') = \left(1 - \frac{\varepsilon^2}{2}\right)\Psi_0(R) + \varepsilon\, i\, \Psi_2(R)$$

where Ψ_0 is the TEM_0 mode (defined with respect to the *undistorted* arm cavity) , Ψ_2 is the TEM_2 mode, and

$$\varepsilon = \frac{\pi w^2 \Delta}{2\lambda R}$$

where Δ is the fractional change in ROC and w is the beam spot at the ITM[1]. Each round trip across the recycling cavity thus diverts light to the TEM_2 mode (relative to the arm) and represents an amplitude loss.

Thus we have $r_l = 1 - \left(\frac{\pi w^2 \Delta}{2\lambda R}\right)^2 \sim 99.5\%$ for $\Delta = 0.3$

where r_l is the TEM_0 mode reflectivity from the ITM.

The recycling cavity loss is of order 1.5 % (the amplitude transmission of the RM). *A* loss from this process greater than 0.5 % will have a significant impact on the stored power. We see from table 1 that we can neglect the deformation of the RM and instead focus on the ITM.

3.2.1. Carrier field

It is interesting that the carrier field suffers almost no distortion from traversing the ITM, for the following reason. The field returning from the arm cavity is composed of 2 parts, the directly reflected field and the cavity leakage field (see figure 2).

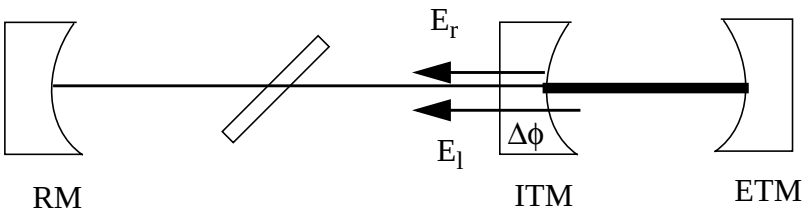

Figure 1:

Thus we have:

$$E = E_r\, e^{2i\Delta\phi} + E_l\, e^{i\Delta\phi}$$

1. Alignment of resonant optical cavities, D. Anderson, Applied Optics, V 23, p. 2944, 1984

where $\Delta\phi$ is the phase change of the light encountered in traversing the distorted ITM, which the reflected field sees twice (input and output) and the leakage field sees once (output). For a low loss arm cavity, we also have:

$$E_l \sim (-2)E_r$$

so that, for small $\Delta\phi$, we obtain:

$$E \sim -E_r$$

and the effect of the ITM distortion is cancelled.

3.2.2. Sideband field

In this case the reflected sideband field sees the distortion of the ITM and suffers a change in wavefront curvature of $\Delta \sim 35$ % (table 1.) From section 3.2, this results in a 0.5 % additional sideband loss in the recycling cavity. The net sideband amplitude transmission to the dark port is then given by:

$$E_{sb} = \frac{t_R^2 E^0{}_{sb}}{2(1 - r_R r_l)} \sim 0.7 E^0{}_{sb}$$

where E^0_{sb} is the sideband field at the dark port with no thermal lensing. This gives a drop in the recycling gain of 50%. The interferometer sensitivity can be written as

$$S/N \sim \frac{E_{sb} E_c}{\sqrt{E_{sb}^2 + P_{ex}}}$$

Here P_{ex} is the excess power present at the dark port, of the order of 200 mW. For $E_{sb}{}^2 > P_{ex}$, the signal to noise is a weak function of E_{sb}. However, for $E_{sb}{}^2 > P_{ex}$, the sensitivity falls linearly with E_{sb}. The above numbers gives $E_{sb} \sim P_{ex}$, so that a 15% loss of sensitivity is obtained.

Coating losses of 6 ppm would give $l \sim 10\%$, resulting in $E_{sb}{}^2 \sim 40$ mW, so that the interferometer sensitivity would drop by a factor 2.

3.3. FFT Simulations

An FFT model of the initial LIGO ifo has previously been used to study the effects of mirror imperfections[1]; finite optic size apodization[2] and mirror radius of curvature tolerance[3] on the complete shot noise performance. Here we report results of an extensive study of thermal lensing effects using a simplified code parameterization. We saw in 4.1 that arm cavities are insignificantly distorted from their design parameters. This, plus carrier insensitivity to the bulk effect (4.2.1), allows us to use the results of earlier FFT studies[1,2,3] to establish the correct $G_{carrier}$ (and corresponding ~critical RM reflectivity) for calculating the intra cavity power levels of table 1 and thus the lensing distortions. This correct G_{cr} is taken, in this sense, equal 50 apriori for these stud-

ies. The main body of FFT runs discussed here had identical arm cavities. Only in 4.3.5 are differential effects investigated.

3.3.1. Thermal Distortion Maps

The surface deformation and OPD effects of mirror beam heating have been previously analyzed[4]. We use these results, scaled to G_{cr}=50, directly. The specific mirror properties assumed are bulk silica absorption =5ppm/cm, and HR coating absorption =0.6ppm. Both these quantities are assumed to apply uniformly across the mirrors. The beam is assumed to be Gaussian and centered on the optic. Thus the distortions modeled are exactly cylindrically symmetric (excepting the BS as discussed below) with respect to the ifo beams. Figure 2 illustrates one portion of one of these distortions (for the ITM). This includes the effect of both coating and bulk absorption heating via the dn/dT effect only. (There is another, much smaller, piece to the net ITM transmission OPD, proportional to (1-n), due to thermal expansion deformation of each substrate surface.) We immediately note

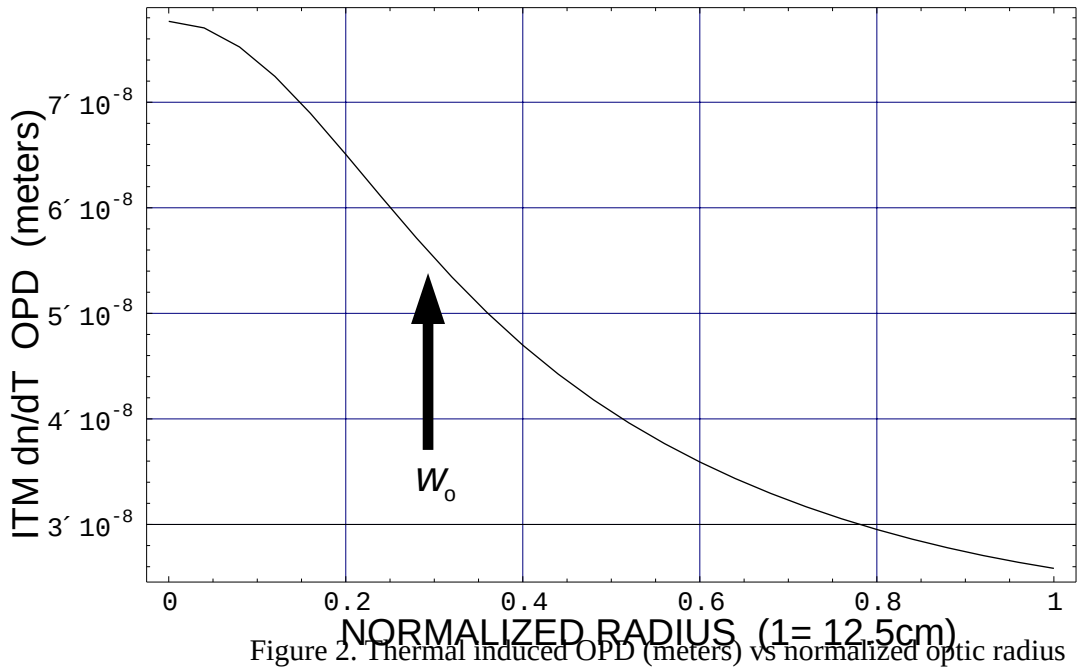

Figure 2. Thermal induced OPD (meters) vs normalized optic radius

that over ~2w_o this OPD is ~30% of the sagitta of the nominal ITM, and that the shape of the distortion is not very well approximated over this span by a simple spherical shape (so that we can not necessarily expect that this distortion would be nearly compensated by a refocusing of the cavity optics). Table 2 summarizes this situation in terms of Zernike polynomial decomposition (e.g $2Z_2$ is the sagitta of the best fit sphere over the fitting radius).

Table 2: decomposition description of Fig. 2 deformation (in nano-meters)

fit radius cm	*ITM design* Z_2	*Deformation shape*						
		Z_2	Z_4	Z_6	Z_8	Z_{10}	*rms*	*PV*
12.5	-268	-17.4	10.9	-5.97	3.89	-2.4	11.5	51.4
w_o	-14.5	-7.24	0.46	-.015	0.0002	0.0	4.23	14.4
$2w_o$	-58.1	-16.8	4.53	-0.67	0.046	-.0.0012	9.92	34.8

Since all the thermal effects have shapes similar to that of Fig 2 we compare all the various distortions which LIGO will nominally experience in table 3. The shaded entries are the effects which are explicitly included into FFT phase distortion maps, the others being regarded as negligible. Note that a couple of the RM entries are large (partly since higher bulk absorption, ≥ 15 ppm/cm, silica will be used) but we neglect them since they are outside of the cavities. The factor two spread in BS entries reflects the uncertainty in the *effect* of the BS distortion. The BS transmission distortions influence only one arm and are thus not “common mode”, so that a factor 1/2 may legitimately be applied for comparison.

Table 3: Summary table of relative thermal distortion amplitude

Optic	*dn/dT*		*Thermo-elastic*		
	Bulk heating	*Surface heating*	*Bulk heating*	*Surface heating*	*dR/R*
ETM	-----	------	-------	.03 G	.004
ITM	= 1 A	.8 B	.05 C	.03 D	.0025
BS	.3 - .6 E	.006 - .012	.01 - 02 F	< .0002	~0
RM	.06 - .012	.012	.006 -.012	< .001	

3.3.1.1 Map construction prescription

These 7 significant distortions (A-G) are converted to Zernike polynomial (through Z_{10}) approximations and then reduced to 5 FFT “phase distortion maps” (pdm) as follows:

1. The ETM surface reflection pdm is generated by the utility zfit which pixilates (over the appropriate grid for the FFT code) the deformation G Zernike terms. However this will effectively change the radius of curvature of the ETM. With a view to compensating such a curvature we subtract the appropriate $Z_{2,eff,G}$ term from the pdm via the “bounce” procedure (see 4.3.1.2). This allows the ETM radius of curvature parameter in the FFT runs (and its polishing specification) to remain the design value = 7400 meters.

2. The ITM surface reflection pdm is generated by zfit using the D Zernike terms. A bounce procedure value $Z_{2,eff,D}$ = 4nm is determined but not subtracted from the pdm. Instead, the ITM reflective surface radius of curvature parameter for the code is changed by

$$\Delta R_{ITM}/R_{ITM} = -\frac{(Z_{2,D} + 3.11 Z_{2,G})}{Z_{2,ITM}} = -.0267$$

this is precisely the amount which compensates the effective curvatures of both arm cavity mirrors so that the Guoy phase of the arms is not changed from the nominal design.

3. An ITM transmission pdm is similarly generated using A+B +2(n-1)C +(n-1)D Zernike terms. No Z_2 subtractions are made from this pdm.

4. The surface reflection from the BS is generated with F Zernike terms. However an attempt is made to approximate the effect of the 45^o angle of incidence. For this an auxiliary Zernike function F' is generated from F by appropriately scaling the radius and values by root 2 (see asymZ.nb routine) which will represent deformation in the diametrical plane of reflection. The average of F and F' is then used to give a final set, Z_2 - Z_{10}, of symmetrical coefficients and the difference a astigmatic set Z_{22} - $Z_{2,10}$. These final sets are then used, via zfit, to generate the tilted BS surface reflection pdm.

5. A similar 'astigmatizing' procedure to that in 4. is done to the E Zernike function. This E, E' set is then generates a zfit pdm which is combined with 2(n-1) times the final pdm of 4 to yield a tilted BS transmission pdm. Here the proper (non-normal) beam path length through the BS is used to calculate absorption, however the non-cylindrically symmetric nature of the heating itself is not taken into account.

3.3.1.2 Bounce procedure

In practice there are only two mirror imperfections which can be compensated for. First is overall tilt, which is automatically compensated by the mirror suspensions via the ASC feedback. Second is a properly defined effective deviation of curvature from the design values[2]. in this case the optic (or in general some other in the same cavity) can be polished to a compensating nominal curvature. As table 2 illustrates, the curvature term (Z_2) of an arbitrary deformation is not a good measure of its effective curvature since it is not invariant with fit radius. For Gaussian beams the proper definition of $Z_{2,effective}$ is had by examining the modal decomposition of a Gaussian beam (LG_{00}) "bounced" off the deformed surface (or transmitted through the OPD distortion). A routine mirror_bounce.f does just this. A pure Z_2 deformation couples LG_{00} only to LG_{10} (LG = Laguerre-Gauss, so that LG_{00} = the pure TEM00 beam). Hence the bounce procedure is to add to the pdm trial $Z_{2,eff}$ until the resultant map when subjected to mirro_bounce.f gives a result with no LG_{10} component in the modal decomposition. When this is performed the other coefficients in the decomposition remain unchanged.

3.3.1.3 FFT runs

A study of the 4000m arm LIGO ifo was conducted using the five pdms of section 4.3.1.1 as the only core optics distortions. The uniform HR 'base' losses and reflectivity of the RM were held

fixed throughout to give an approximately realistic G_{cr} = 72. It is remarkably confirmed throughout all the runs to be discussed here that G_{cr} varies by < 1%. The construction of the five pdms is consistent with a fabrication strategy that all surfaces be polished to the nominal design values[2] with the exception of the HR RM and ITM radii of curvature. R_{ITM} is adjusted in the runs by the compensation described in 4. of section 4.3.1.1. Then R_{RM} is varied (run to run) to find a value which optimizes side-band performance (typically taken as maximizing $G_{sb,00}$). See Appendix 1 for the full run parameterization.

Since the Schnupp asymmetry is usually the largest source of side-band light loss, but here we want to study thermal lensing and compensations, we hold it fixed throughout at a value typical for LIGO models with no lensing. This sets $G_{sb,max}$= 47.5, which is obtained for running with no lensing pdms (confirmed by simple analytic TEM_{00} resonance calculation).

A summary of this FFT run study is shown in figure 3. The nominal design R_{RM}= 10008 m is marked by the thick abscissa line. Curve 1 are FFT runs with *each* pdm map having Z_2 subtracted according to the bounce procedure. Thus we might expect that a pure Z_2 compensation, as by varying R_{RM}, would give maximum gain at the nominal. Instead the maximum G_{sb} occurs at R_{RM}

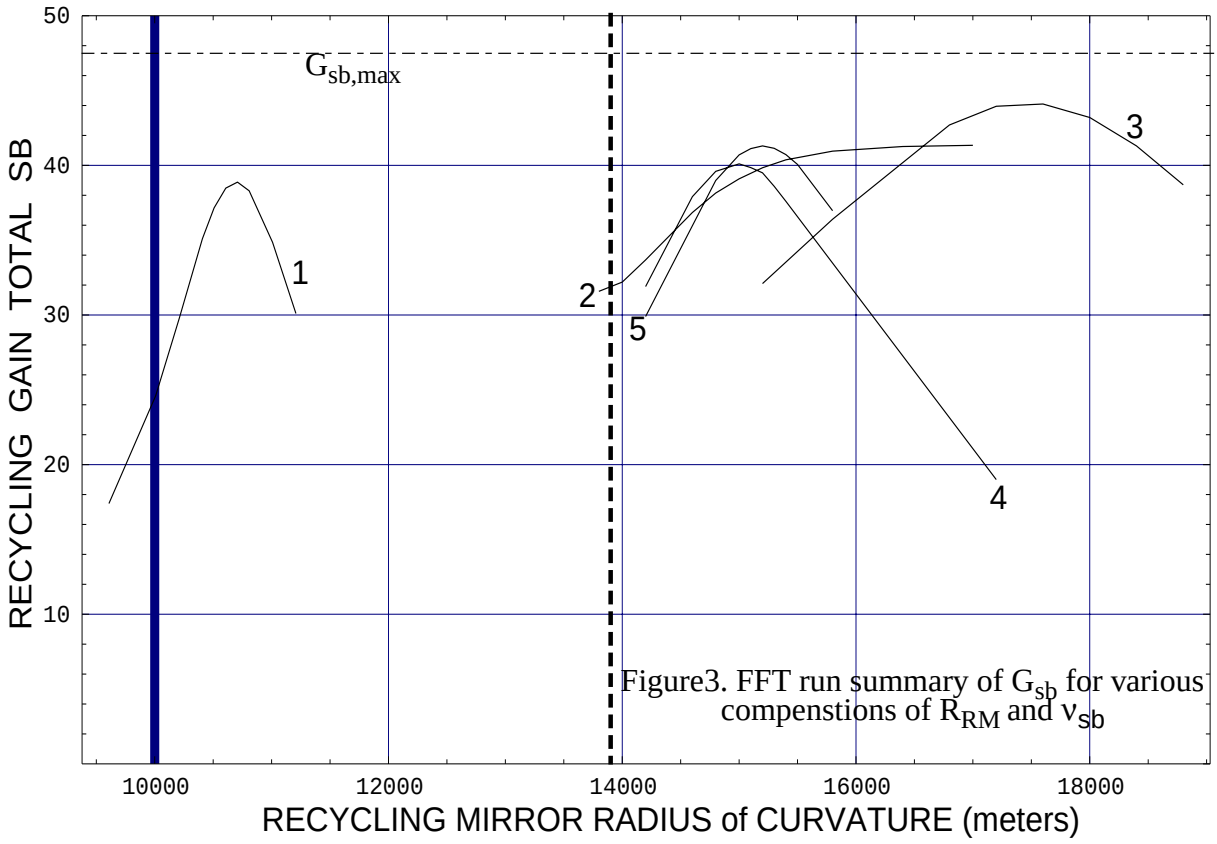

Figure3. FFT run summary of G_{sb} for various compenstions of R_{RM} and ν_{sb}

increased by 6.5%. The curves 2-6 are with the pdms described in 4.3.1.1, differing only in how the SB modulation frequency is fine tuned for the run sequence. Curve 2 are runs where ν_{sb} is optimized for each run (value of R_{RM}). This is the standard mode of FFT running and the range of ν_{sb} change over curve 2 is ~ 6kHz. Note that changes of R_{RM} within the entire range studied here cause resonant optimization of the cavity lengths of at most a few 10^{-11} meters, so that far less than ~1 Hz ν_{sb} changes are expected. For actual LIGO operation a fixed ν_{sb} would be chosen so the runs of curve 5, where ν_{sb} = the exact recycling cavity resonant value for the nominal cavity lengths (see parameters of Appendix 1). Curves 3 and 4 are then for ν_{sb} fixed but at values +3300 Hz and -1000 Hz offset from this exact nominal resonant value.

To confirm that the TEM_{00} SB field component behaves in the same way, figure 4 reproduces the same curves for that component.

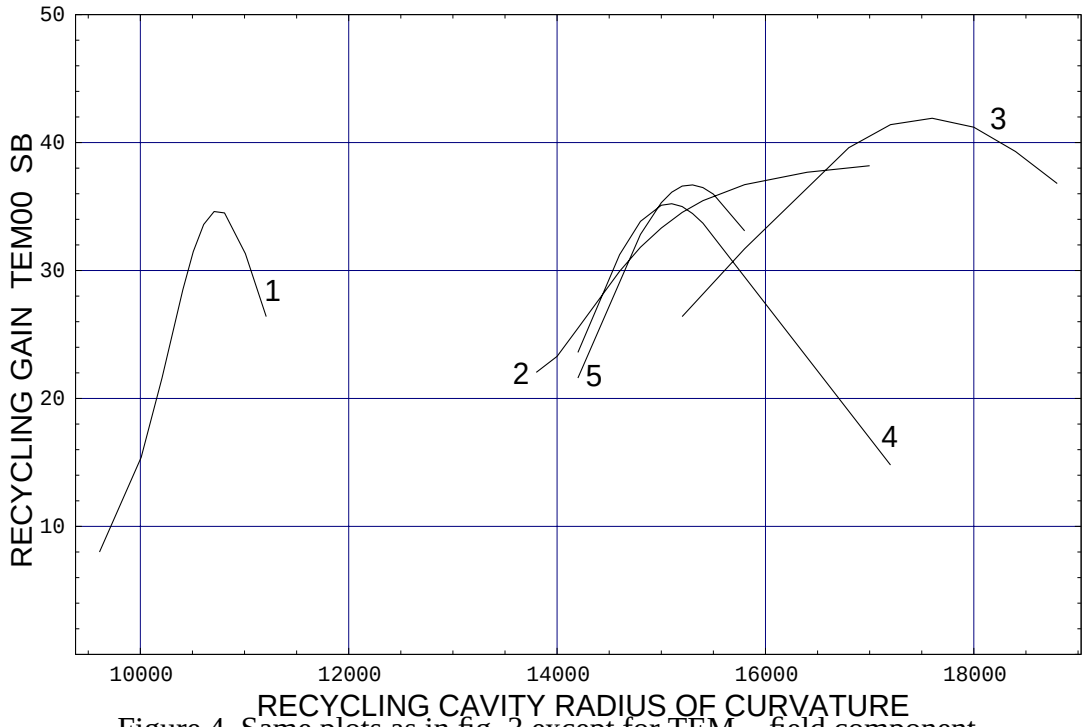

Figure 4. Same plots as in fig. 3 except for TEM_{00} field component

From the bounce procedure $Z_{2,eff}$ values for each pdm we can estimate the total optical power (focusing) which the net lensing introduces in the recycling cavity. To compensate for introducing such a pure power, R_{RM} would have to equal 13900 m, indicated as the dashed abscissa line in Fig. 3. The actual compensation, as given by the peak of curve 5 for example, is about the same percentage higher as the Curve 1 was with respect to nominal (the solid abscissa). This additional compensation is characteristic of non-spherical distortions. Equivalent compensation procedures to that described in this section have been performed where the pdms were pure spheres or tilts. Then it was found first, that all curves like 2-5 collapse to ones with a common peak, and second that the peak of 1 and of 2-5 lie exactly on the solid and dashed expectations.

3.3.1.4 EFFECT ON STRAIN SENSITIVITY

Although the SB gain is quite sensitive to thermal lensing, its effect on overall shot noise strain sensitivity is not direct or obvious. For a given thermal lensing SB degradation, the Schnupp asymmetry and the SB modulation factor (Γ) can be reoptimized to partially compensate. The same body of FFT run results is presented in terms of relative shot noise strain sensitivity (h_{100}) in figure 5. The discussion of section 3.3.1.3 concerned runs with thermal lensing corresponding to $\mathbf{P}_{\text{incident}}$= 6 Watt (points in Fig 5 intersecting the 6 W line). Runs were extended to other $\mathbf{P}_{\text{incident}}$ values by simply scaling the FFT thermal lens phase maps proportionally to $\mathbf{P}_{\text{incident}}$. Each point in figure 5 has been optimized with respect to Γ and Schnupp asymmetry. Each curve corresponds to a different RM curvature compensation. Curve 1, for instance, has no compensation (R_{RM}= 10008m) so that its value at $\mathbf{P}_{\text{incident}}$= 0 is unity, by definition. Curve 3 corresponds to the optimum R_{RM} = 14900m compensation for $\mathbf{P}_{\text{incident}}$ = 6W, as determined from the peak of curve 5 of figure 4. Curves 2 and 4 are similarly optimum R_{RM} compensation for $\mathbf{P}_{\text{incident}}$= 3W and 8W respectively (R_{RM} = 12000m and 17700m). Over the points of Fig. 5, the Schnupp asymmetry varies from 11 to 35 cm (precisely the “unbalancing length”: see appendix 1) to achieve optimization, and Γ ranges from 0.26 to 0.44.

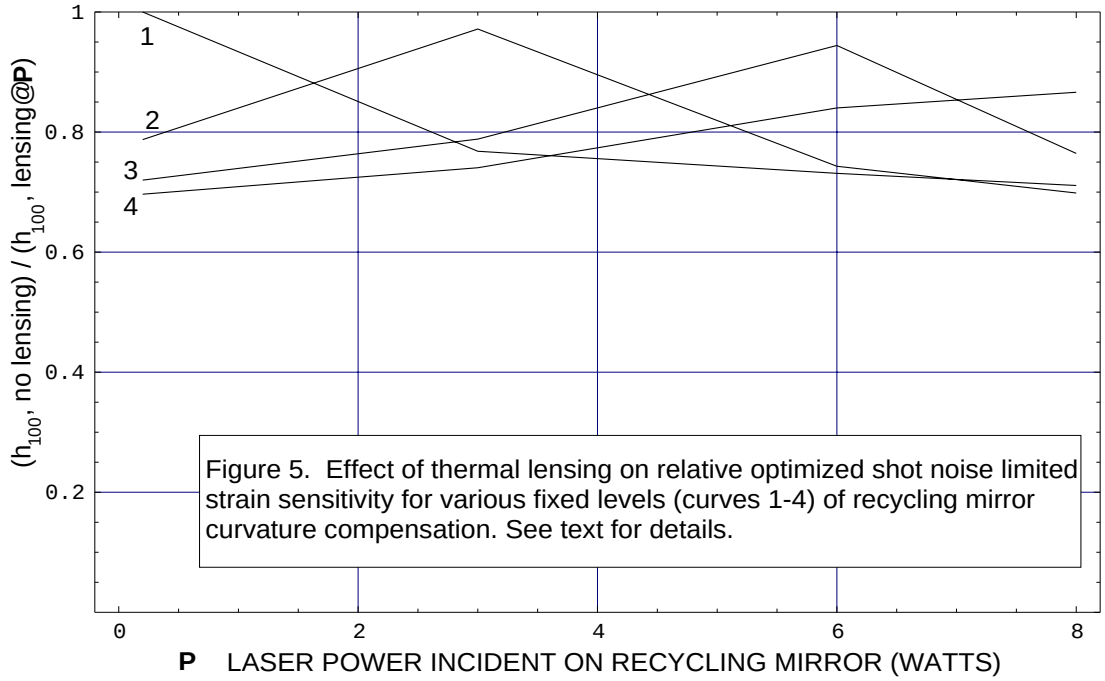

Figure 5. Relative compensated strain sensitivity. Each curve is strain sensitivity relative to the zero power incident point of curve 1 for various RM curvature compensated powers.

4 SUMMARY

We summarize the results of this note:

- Distortion of the core optics through absorption of light is most severe for thermal lensing of the ITM
- The coupling of the arm and recycling cavities leaves the carrier largely unaffected by ITM distortion
- Sideband power at the dark port is degraded by ~50% for the following loss levels, each contributing about equally to the ITM thermal lensing, leading to a ~ 15% sensitivity change:
  - 5 ppm / cm bulk
  - 0.6 ppm coating
- Compenstation of the ITM lensing is possible by changing the radius of curvature of the RM by ~ 40% to match the distorted ITM
  - Further compensation is possible through the tuning of the sideband frequency. This effect is not fully understood

An increase of coating loss to 6 ppm on the ITM would give a sensitivity loss of a factor 2 with no RM radius of curvature compensation

5 REFERENCES

1. The FFT code version used here is the parallel PARAGON supercomputer version c. 6/96 by B. Bochner, the culmination of extensive development by B. Bochner and Y. Hefetz. Previous studies of the effects of mirrors with deformed polished surfaces for a 514.5 nm ifo are in B. Bochner, LIGO-G950061-R (8/29/95). More recent work at 1064 nm with the PARAGON version are partially described in S. Whitcomb, et. al, LIGO-P960044-00-D (9/96),and W. Kells in LIGO- (12/96 LIGO Science and Integration meeting notes).

2. The Core Optics Components DRD, LIGO-E950099_04-D.

3.”COC Surface Radii Tolerances, Bill Kells, LIGO-T960014-00-D (8/96).

APPENDIX 1 FFT RUN PARAMETERIZATION

Wavelength of the laser (all lengths are in meters): 1.064D-06

Index of refraction for mirror substrates (depends upon Wavelength & Materials): 1.44963

Base laser modulation frequency (Hz), initial del mod. freq. (Hz), Adjust Sb Freq? (Y=1,N=0, fixed lengths only): -24000874.7d0 000.0d0 1

Base Lengths L1, L2, L3, L4, L5: 4.999999872 4.189999656 4.189999656 4000.2103834 4000.2103834

Unbalancing length to add to L2 and subtract from L3 (Only used for Lenchange runs, no Asymm. optim.): .11d0

Bring exact lengths to resonance (1) or read fixed lengths from data file (0)? 0

Data file to (write/read) resonant lengths & params (to/from):(max 38 chars)

res_val_unbal.dat

Read from/Do (for lenchange/fixedlen case) Asymm. Length Optim. Run (Y=1,N=0)?

0

Mirror Radii of Curvature (Reflective-side curvature, >0 is Refl-Side Concave,

USE “1.11d+15” to mean “FLAT”) for Mrecyc, Mft, Mfr, Mtback and Mrback:

variabled0 14400.d0 14400.d0 7400.d0 7400.d0

CARRIER Beam Spot Size, Curvature-Radius, at ON-LINE FP-Input Mirror:

(USE “1.11d+15” to mean “FLAT”; Curv.Rad.>0 means waist INSIDE On-line Arm Cav):

3.6343d-2 23000.0d0

Width of square calculational window:

0.35

Radius of diaphragms on Mrecyc, Mft, Mfr, Mtback, Mrback, Mbs(x-dir),Mbs(y-dir):

.120 .120 .120 .120 .120 .086 .122

Propagator Momentum-Space Cutoff & Apodization Info, for Anti-Aliasing:

Highest P-Space Pixel With No Aliasing (Prop1,Prop2,Prop3,Prop4,Prop5)

1000 1000 1000 9 9

Highest P-Space Pixel With Real Physics (Prop1,Prop2,Prop3,Prop4,Prop5):

1000 1000 1000 25 25

Initial Reflectivity of Mrecyc, Preliminary DelRef1, Optimize(lenchange runs)/Use Optim Results(fixed len’s)? (Y=1, N=0) 0.98371975 0.0 0

Base REF-Side Intensity Reflectivities -- Mft, Mfr, Mbs, Mtback, Mrback:

0.97d0 0.97d0 0.5d0 0.99995d0 0.99995d0

Some Base Anti-Reflection-Side Intensity Reflectivities -- Mft, Mfr, Mbs:

0.97d0 0.97d0 0.5d0

Base REF-Side Losses in mirrors Mrecyc, Mft, Mfr, Mbs, Mtback, Mrback:

5.0D-5 5.0D-5 5.0D-5 .0D-5 5.0D-5 5.0D-5

(Note that Transmission T is made to satisfy: T_AR-side=T_REF-side, and T+R+L=1)

Postion & angle error of excitation laser beam: dx,dy,theta(microrad),phi(deg)

Position & angle error of mirror Mrecyc; dx, dy, theta(microrad), phi(deg)

Postion & angle error of mirror Mft; dx, dy, theta (microradians), phi (deg)

Postion & angle error of mirror Mfr; dx, dy, theta (microradians), phi (deg)

Position & angle error of mirror Mtback; dx, dy, theta(microrad), phi(deg)

Position & angle error of mirror Mrback; dx, dy, theta(microrad), phi(deg)

All 0.0d0 0.0d0 0.0d0 0.0d0

Position error for Beamsplitter; dx (short axis), dy:

0.0d0 0.0d0

Base thicknesses (in meters of substrate) of mirrors Mrecyc, Mft, Mfr, Mbs :

0.0d0 0.10d0 0.10d0 0.04d0

Binary Orientation of Beamsplitter (1 if Ref. Coating faces On-Line Cav., 0 if Ref. Coating faces Off-Line Cav.): 0

Maximum # of relaxation iter's, and max. integ. errors (recycling cav, cav4,5):1000 6.0D-5 1.3D-4 1.3D-4

Mirror Specification Section: (max 38 characters for all mirror filenames!)

Names of the files containing mirror PHASE variations:

Reflections from the reflective side:

(Codes: "+" = all zeroes)

Recycling Mirror :+

On-line input mirror : surfITM.dat

Off-line input mirror : surfITM.dat

On-line FP back mirror : surfETM2.dat

Off-line FP back mirror : surfETM2.dat

Transmissions:

(Codes: "+" = all zeroes)

Recycling Mirror :

+

On-line input mirror :

transthermITM.dat

Off-line input mirror :

transthermITM.dat

Reflections from the anti-reflective side (minus sign automatically included):

(Codes: "+" = all zeroes, "-" = Make Phase[Conj[R_antiref]] = pi + Phase[R_ref*(Conj[t]/t)])

Recycling Mirror : -

On-line input mirror : -

Off-line input mirror : -

Beamsplitter Phase Maps: (Code #1: “+” = all zeroes)

Reflection from reflective side:

surfBS.dat

Transmission from reflective side:

transthermBS.dat (Codes #1,#2: “+”, “=” = Same T map as from Refl. Side)

Transmission from anti-reflective side: =

(Codes #1,#3: “+”, “-” = Make Phase The Appropriate Conjugate of the Other R’s & T’s)

Reflection from anti-reflective side: -